A&A 386, 204–210 (2002)
DOI: 10.1051/0004-6361:20011387

Astronomy & Astrophysics

Discovery of X-ray emission from the protostellar jet L1551 IRS5 (HH 154)

F. Favata[1], C. V. M. Fridlund[1], G. Micela[2], S. Sciortino[2], and A. A. Kaas[3]

[1] Astrophysics Division – Space Science Department of ESA, ESTEC, Postbus 299, 2200 AG Noordwijk, The Netherlands
[2] Osservatorio Astronomico di Palermo, Piazza del Parlamento 1, 90134 Palermo, Italy
[3] Nordic Optical Telescope, Apartado 474, 38700 Santa Cruz de la Palma, Canarias, Spain

Received 20 July 2001 / Accepted 27 September 2001

Abstract. We have for the first time detected X-ray emission associated with a protostellar jet, on the jet emanating from the L1551 IRS5 protostar. The IRS5 protostar is hidden behind a very large absorbing column density, making the direct observation of the jet's emission possible. The observed X-ray emission is likely associated with the shock "working surface", i.e. the interface between the jet and the circumstellar medium. The X-ray luminosity emanating from the jet is, at $L_{\rm X} \simeq 3 \times 10^{29}$ erg s^{-1}, a significant fraction of the luminosity normally associated with the coronal emission from young stars. The spectrum of the X-ray emission is compatible with thermal emission from a hot plasma, with a temperature of $\simeq$4 MK, higher than the temperature expected (on the basis of the jet's velocity) for the shock front produced by the jet hitting the circumstellar medium.

Key words. ISM: clouds – ISM: individual objects: L1551: HH 454– ISM: jets and outflows – stars: formation – stars: pre-main sequence – radio lines: ISM

1. Introduction

During the final stages of the formation of low-mass stars (in the so-called classical T Tau phase) accretion of material from the proto-stellar nebula onto the Young Stellar Object (YSO) takes place through an accretion disk. Very often (and possibly always) the presence of the accretion disk is correlated with the presence of energetic polar outflows, that is, collimated jets of material being ejected perpendicularly to the disk, along its axis. Several models of the formation of the jet have been proposed, in most of which the jet is collimated by the presence of a (protostellar) magnetic field. When these jets collide with the surrounding ambient medium – or with previously ejected material – they form a shock structure, which is directly observable in the form of so-called Herbig-Haro jets (e.g. Reipurth & Raga 1999).

X-ray emission (and thus the presence of hot plasma, at temperatures in excess of several $\times 10^5$ K, up to $\simeq$100 MK during energetic flares) has by now been observed in most stages of the formation of low-mass stars, ranging from the highly embedded, perhaps spherically accreting protostars (Class 0 objects) to the final stages of the pre-main sequence life of a star, the Weak-Line T Tau stage, during which the X-ray luminosity is thought to come from a "normal" (however very active) stellar corona.

While accretion itself has been considered as a possible source of X-ray emission in classical T Tau stars, up to now no evidence of energetic phenomena associated with protostellar jets has been observed. In this paper we present the first observations of X-ray emission from a protostellar jet, obtained in a well-studied system in which the proto-star (and its immediate circumstellar environment) powering the outflow is so heavily obscured that the jet can be singled out as the source of emission of the X-rays without ambiguity. Our observations show that this jet is indeed an X-ray source with a luminosity equivalent to a fraction of the X-ray luminosity normally associated with YSOs. The observed X-ray spectrum is compatible with a thermal origin of the observed X-ray emission. The associated temperature is moderate, but higher than expected on the basis of the shock velocities observed in this and other Herbig-Haro jets. This raises the question of whether the X-ray emission associated with jets could indeed be a common feature of stellar formation, so that

Send offprint requests to: F. Favata,
e-mail: Fabio.Favata@rssd.esa.int

in some cases a significant fraction of the X-ray luminosity associated with the star (YSO/accretion disk) is actually emanating from shocks in the jet.

2. The L1551 IRS5 outflow

The L1551 cloud is one of the nearest ($d \simeq 140$ pc) sites of ongoing star formation, in which objects in several different stages of the process are clearly visible, from deeply embedded, actively accreting (proto-)stars to the final stages of star formation represented by the Weak-Line T Tau stars with no remaining circumstellar material. Several "canonical" examples of jets and outflows associated with protostellar accretion are present in the region. In this paper we are mainly concerned with the jet associated with the IRS5 source embedded in the L1551 cloud and its associated outflow.

L1551 IRS5 is a deeply embedded protostellar binary system (e.g. Rodriguez et al. 1998 and references therein), effectively invisible at optical wavelengths as it is hidden behind some ≃150 mag of visual extinction (Stocke et al. 1988; Smith et al. 1987; White et al. 2000) which most likely originates in the circumstellar accretion disk. The two Class 0/1 stars have a total luminosity of ≃30 $L_\odot$. The two IRS5 stars appear to be (jointly?) powering at least two observable outflows. A large (several arcmin) bipolar molecular outflow (actually the first discovered, Snell et al. 1980) and a much smaller (with a length of ≃10 arcsec) denser two-component jet (Fridlund & Liseau 1998), consisting of material at temperatures of $T \simeq 10^4$ K, thus visible in the emission lines of e.g. Hα, representative of recombination. The jet and the molecular outflow have been shown to be likely causally unrelated, given that the jet has a momentum insufficient by several orders of magnitude to drive the molecular outflow (Fridlund & Liseau 1998). The jet moves at transverse velocity of 200–400 km s^{-1} (Fridlund & Liseau 1994) and appears to end in a shock against the ambient medium (a "working surface" – Fridlund & Liseau 1998)

3. Observations

3.1. XMM-Newton

The X-ray observations discussed in the this paper were obtained with the XMM-Newton observatory. A deep (50 ks) exposure of the star-forming region of the L1551 cloud was obtained starting on Sep. 9 2000 at 19:10 UTC. All three EPIC cameras were active at the time of the observation, in full-frame mode, with the medium filters.

Data have been processed by us with the standard SAS V5.0.1 pipeline system, concentrating, for the spectral analysis, on the EPIC-PN camera. In order to minimize the unwanted contribution of non-X-ray events we have retained only the counts whose energy is in the 0.3–7.9 keV range. To deal with the time-varying background, we have applied a technique purposely developed at the Palermo Astronomical Observatory which maximizes the

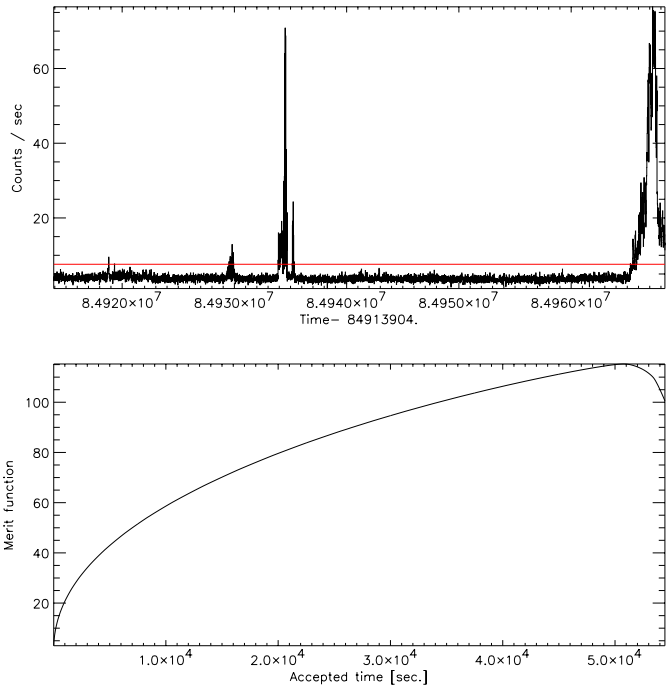

Fig. 1. The top panel shows the total count rate as a function of time in the PN camera during the complete L1551 XMM observation discussed in the present paper. The horizontal line is the chosen threshold value for background filtering: time intervals during which the total PN count rate was above the line have been discarded from the final data set. The bottom panel shows the value of the merit function, as a function of the total accepted observing time, which was used to determine the threshold. The merit function is optimized to yield an optimal data set for the detection of faint sources.

statistical significance of weak sources by identifying and removing the fraction of the exposure time strongly affected by high-background episodes.

In many XMM data sets most of the background is due to a small number of short (but intense) episodes – mostly related to solar events – so that the background events are strongly concentrated in time. Removal of the small fraction of the observing time in which the high-background episodes are concentrated results in a much larger S/N ratio data set with a comparatively small loss of source photons. Figure 1 shows the time evolution of the total count rate for the PN data set (in the top panel), together with the threshold (shown by the horizontal line) above which the data are discarded. The threshold is dynamically chosen by maximizing a merit function, defined to optimize the detection of faint sources (which are background, rather than photon-noise, dominated). The value of the merit function for the L1551 PN observation is plotted in the lower panel of Fig. 1 as a function of the total accepted time.

As a result of the overall procedure the initial data set of ≃10^6 photons collected during an exposure of ≃56.8 ks for the MOS cameras and ≃54.5 ks for the PN camera, was reduced to a cleaned data set of ≃250 000 photons collected in ≃55 ks for the MOS and ≃51 ks for the PN

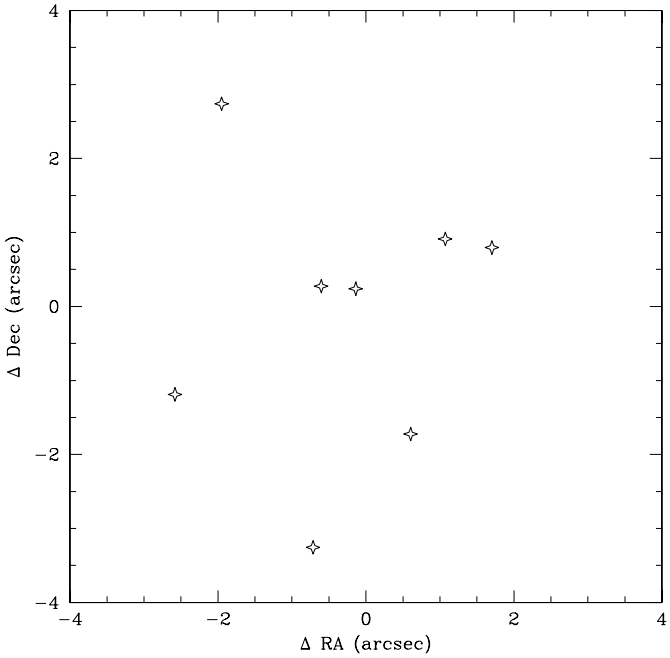

Fig. 2. The plot shows the difference (in arcsec) between the coordinate of the X-ray source as determined in the PN detector by the PWDETECT algorithm and their optical counterpart, for the 8 bright X-ray sources (with more than 300 counts) with unambiguous counterparts in the L1551 XMM observation.

cameras, i.e with a judicious time and energy filtering we have been able to reduce the background level by a factor $\simeq$4 while rejecting only $\simeq$5% of the overall exposure time.

The cleaned data set obtained by summing the data of the two MOS and one PN EPIC cameras has been searched for sources with the Wavelet Transform detection algorithm also developed at Palermo Astronomical Observatory (PWDETECT, Damiani et al. 2001 in preparation). The characteristics of the XMM-Newton version of the algorithm are inherited from the version developed for the ROSAT PSPC (Damiani et al. 1997). The overall analysis procedure follows the recipe described in more details by Sciortino et al. (2001). The L1551 observation has been taken with the medium filters; in such a case we have derived that the value of the relative efficiency of the PN and of the individual MOS cameras is 2.94, hence the summed data set has a single MOS-equivalent cleaned exposure time of $2 \times 55 + 2.94 \times 51 = 260$ ks.

In order to assess the source significance threshold to adopt to ensure detection of the faintest sources a full set of simulations of empty fields with the same background level and the same exposure map as the summed data set needs to be run. Following this, a limiting threshold can be set which ensures e.g. a maximum of one spurious source per field. While this has been done for the complete analysis of the full L1551 exposure (and will be discussed in a future paper), the three X-ray sources discussed in the present paper are all well above the minimum threshold, and consequently their significance is well above the spurious source threshold.

The quality of the XMM aspect solution ("bore-sight correction") was verified by comparing the positions of X-ray bright sources as determined in the PN detector by the PWDETECT algorithm with the position of their optical counterparts. Only X-ray bright sources (with more than 300 source counts in the PN camera) with single, unambiguous optical counterparts with good position determination were used, resulting in 8 such sources being available in the L1551 field. The optical coordinates were obtained from the SIMBAD database. No significant bias is present in the data, with a mean ΔRA $= -0.33 \pm$ 1.46 arcsec, and a mean ΔDec $= -0.15 \pm 1.85$ arcsec, so that the positional error for the faint sources is fully dominated by the photon noise coupled with the XMM point spread function.

The extraction of source and background photons was performed using the XMMSELECT tool. Source photons have been extracted from a circular region of 45 arcsec diameter, while background photons have been extracted from a region on the same CCD chip and at the same off-axis angle as for the source region. Response matrices ("ARF files") appropriate for the position and size of the source extraction regions have been computed for the EPIC PN camera. The spectral analysis has been performed using the XSPEC package, after rebinning the source spectra to a minimum of 20 source counts per (variable width) bin.

3.2. Ground-based observations

New optical spectra and images of the IRS5 jet have been obtained with the 2.6 m Nordic Optical Telescope (NOT). The spectra were obtained in December 1999 using the echelle mode of the ALFOSC combined imager and spectrograph. The cross disperser/grating combination allowed for a spectral resolution of $\simeq$1 Å at the wavelength of Hα. The detector was a 2048×2048 15 μm pixel CCD. A slit width of 1 arcsec projected on the sky was used, and the integration time per spectrum was 3600 s. The complete velocity field of the jet was mapped in emission lines between 4800 Å and 7900 Å. For the purpose of evaluating shock velocities in this paper our interpretation is based on an analysis of the Hα data with the other lines used as a consistency check. A full analysis will be presented in a forthcoming paper. Hβ was used together with Hα in order to estimate the extinction towards the shocks in the L1551 IRS5 jet.

For the identification of the optical counterparts to the X-ray sources detected in the XMM image both new narrow band images (also obtained with the NOT) and already available HST images were used. The HST R-band WFPC2 image of the jet region is shown in Fig. 3 together with the EPIC PN X-ray image; the position of the X-ray source associated with the L1551 jet, together with the position of one of the background sources, is shown on

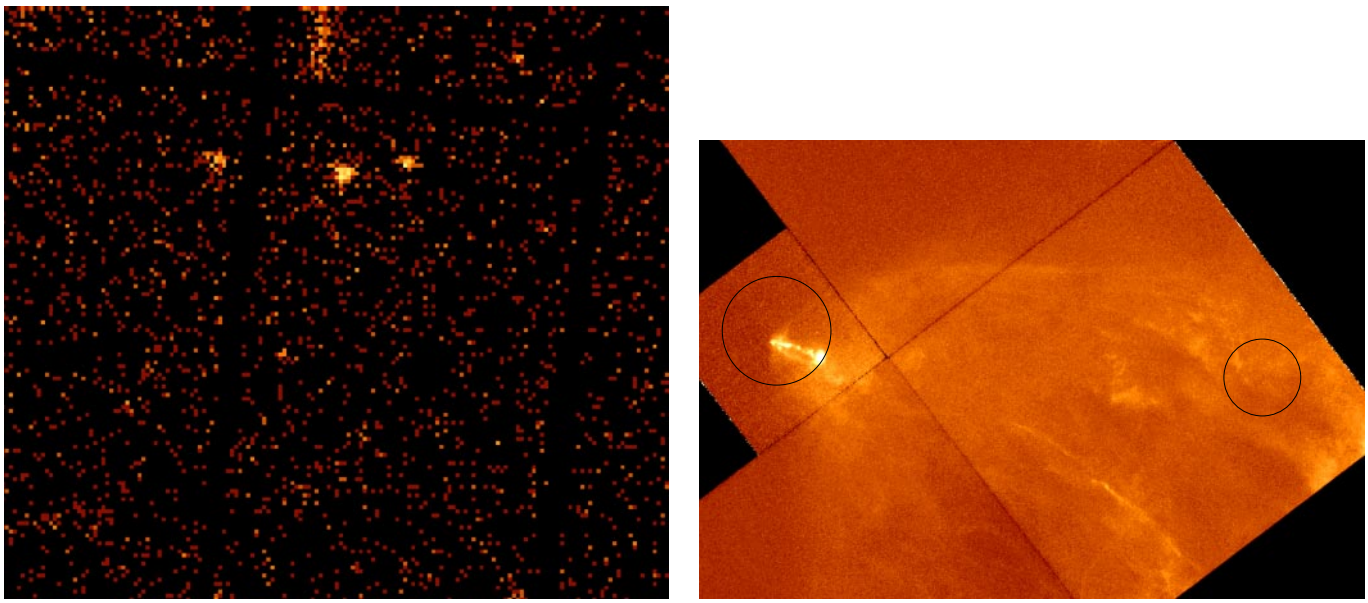

Fig. 3. The left panel shows the region of L1551 IRS5 in X-rays, as seen in the XMM EPIC-PN camera, while the right panel shows a small part of the same region as seen in a 1800 s R-band CCD image obtained with the Hubble Space Telescope WFPC2 camera. The size of the small detector (the WFPC2-PC chip) on the left part of the HST image is 36.8 arcsec, while the size of the X-ray image is 9.3×6.3 arcmin. The position of the two leftmost X-ray sources visible in the left panel is indicated on the R-band image by the circles. The leftmost X-ray point source is the one associated with L1551 IRS5, while the other point source is one of the two background sources discussed in Sect. 5. The nearly vertical alignment of bright pixels near the center-top of the X-ray image is due to "spill-over" from a bright source higher up in the image.

the WFPC2 image by a black circle. The size of the circle corresponds to the likely extent of the X-ray source as determined by the PWDETECT algorithm. The WFPC2 image was obtained in February 1996 with the F675W (R-band) filter, and part of it is discussed in Fridlund & Liseau (1998).

New narrow band images were also obtained with the NOT. These observations were carried out in March 2001 again using the ALFOSC, this time in imaging mode. Deep images integrated for 1800 s (Hα) and 3600 s (I-band) were obtained in order to detect possible new emission knots, as well as to search for faint background or embedded sources shining through the molecular cloud (in possible association with the background X-ray sources discussed in Sect. 5). A narrow band filter centered on the Hα line was used, while the I-band filter was centered on 7150 Å with a FWHM of 1600 Å. Being several arcmin in size, the field of view of the NOT images is significantly larger than the WFPC2 one, although with less spatial resolution and shallower limiting magnitude.

4. X-ray emission from the L1551 IRS5 jet

A faint X-ray source (the leftmost one in the left panel of Fig. 3) is positionally coincident with the embedded source L1551 IRS5 and its jet. The background-subtracted count rate is only 8.4×10^{-4} cts s^{-1} in the EPIC PN camera, so that the total number of source counts is limited to 42 cts in the $\simeq$50 ks exposure (with an equivalent number of background counts in the extraction box used, a circle 45 arcsec in diameter). The low statistics allow a limited amount of spectral information to be derived for the source. The resulting spectrum (shown in Fig. 4) is soft, and can be reasonably described with a moderately absorbed thermal spectrum. Using a MEKAL model with an added interstellar absorption component in XSPEC gives a best-fit temperature $T = 4 \pm 2.5 \times 10^6$ K, with a moderate value of the best-fit absorption ($1.4 \pm 0.4 \times 10^{22}$ cm^{-2}), corresponding to an extinction of $A_V = 7.3 \pm 2.1$ mag[1]. The null hypothesis probability for the fit is 15%, i.e. the fit is, from the statistical point of view, fully acceptable. The limited statistics of the spectrum (and the corresponding small number of bins) do not allow to constrain the spectrum at a more detailed level. The full width at half power (FWHP) of the XMM point-spread function (PSF) for EPIC PN camera is $\simeq$14 arcsec, significantly larger than the size of the jets (whose visible length is $\simeq$10 arcsec). Thus, it is not possible to locate the precise site of the X-ray emission within the jet structure.

5. Background sources

Two additional X-ray source are detected within the area on the sky that is dominated by the molecular outflow from L1551 IRS5. The centroid positions, and background subtracted count-rates can be found in Table 1. The position of the brighter of the two against the molecular outflow is visibile in Fig. 3. Neither of these sources can

[1] Using a conversion factor $N_H/A_V = 1.9 \times 10^{21}$ atoms cm^{-2} mag^{-1}, see e.g. Cox (2000).

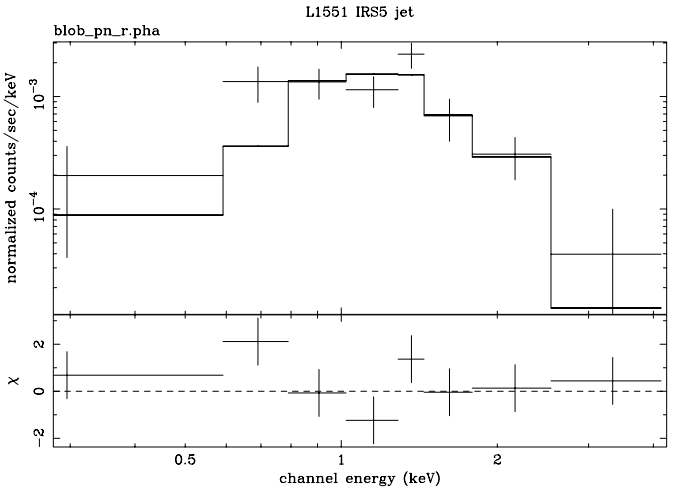

Fig. 4. The observed, background-subtracted EPIC PN X-ray spectrum of the X-ray source associated with the L1551 IRS5 jet. The best-fit thermal ("MEKAL") spectrum – whose parameters are given in Table 1 – is also shown.

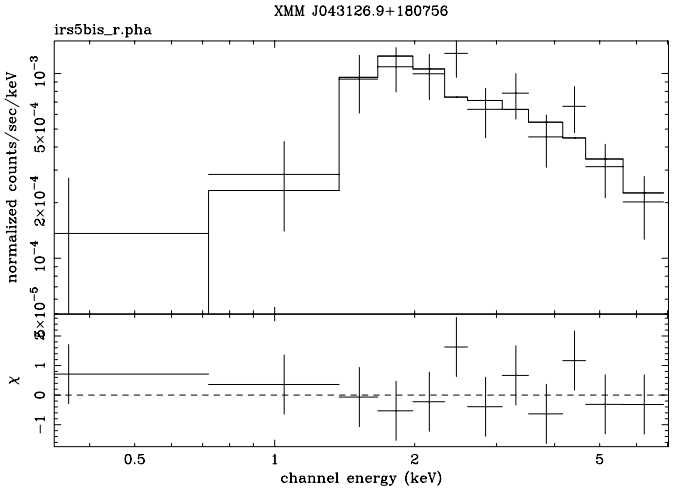

Fig. 5. The observed, background-subtracted EPIC PN X-ray spectrum of the X-ray source XMM J043126.9 + 180756. The best-fit absorbed power-law spectrum – whose parameters are given in Table 1 – is also shown.

be associated with any visible object in the deep Hα and I-band images at these positions.

Both χ^2 and K-S tests show that the X-ray emission from these sources is constant to a high ($\geq$90%) probability level. The spectra of these two sources are significantly harder than the spectrum of the source associated with the L1551 IRS5 jet (the spectrum of the brighter of the two is shown in Fig. 5), and can both be satisfactorily described with an absorbed power-law spectrum, with indices varying between 1.2 and 2.5. The absorbing column density is in both cases moderate, with A_V between $\simeq$5 and $\simeq$8 mag. The resulting column densities are thus similar to what is expected for the L1551 molecular cloud at these positions (Sandqvist & Bernes 1980). Given the X-ray spectral characteristics, as well as the lack of any visible candidate counterpart in our deep I-band images, we consider it likely that these sources are not associated with the molecular L1551 IRS5 outflow, even though they are positionally coincident with (parts of) it. Rather, they are most likely to be extra-galactic X-ray sources (plausibly active galactic nuclei) shining through the L1551 cloud. Typical active galactic nuclei would have, on the basis of their high $F_{\rm X}/F_V$ ratio, optical magnitudes $V \gtrsim 19$, which would become $V \gtrsim 24$ when the intervening column density is taken into account. Therefore their optical counterparts are not expected to be visible, on the optical images presented here, againts the background of the molecular outflow emission.

The spectra could in principle be fit also with a thermal spectrum, with a very high resulting temperature ($T \gtrsim 100$ MK). While this temperature would not be incompatible with coronal protostellar origin during e.g. an energetic flare, the lack of any visible counterpart down to faint magnitudes (even though the absorbing column is only a few magnitudes) and the constant light curve of the sources make this last hypothesis unlikely.

The presence of two serendipitous X-ray sources in the PN image shown in Fig. 3 at flux levels of order 10^{-14} erg cm^{-2} s^{-1} is fully in line with the expected number density of background sources determined on the basis of the $\log N$–$\log S$ relationship for X-ray sources (see e.g. Hasinger et al. 2001), which predicts that at this flux limit 100 to 200 sources per square degree should be present in any given X-ray observation. The area covered by X-ray image of Fig. 3 is $\simeq$0.02 square deg, so that the expected number of serendipitous sources is 2 to 4.

6. Discussion

Hubble Space Telescope (HST) observations (Fridlund & Liseau 1998) indicate the presence of a number of shocks along the extent of the IRS5 jet. The jet is observed to end in a "working surface" against the ambient medium at $\simeq$10 arcsec from the presumed location of the source powering it (see Figs. 1 and 2 of Fridlund & Liseau 1998). This shock feature is designated "knot D" in the nomenclature of Neckel & Staude (1987) and Fridlund & Liseau (1994). We have measured the Hα/Hβ ratio towards the working surface (knot D) of the jet. Assuming a type B pure recombination spectrum (which is justified since we also detect [O III] 5007 Å emission at this position – see below), we find A_V to be 4–6 mag, depending on which extinction law is applied. We also find that the extinction is increasing in the direction towards IRS5 along the jet (confirming the result of Stocke et al. 1988). The absorbing column density, for the IRS5 X-ray spectrum, is thus compatible with the absorbing column density measured toward the visible jet (and in particular toward the shock feature), making the association between the X-ray emission and the jet plausible. Since as mentioned above the IRS5 protostellar system is hidden behind a very thick layer of absorbing material, corresponding to $A_V \gtrsim 150$ mag, it can be excluded that the X-ray photons – given the small

Table 1. Coordinates, count rates and best-fit spectral parameters for the three X-ray sources discussed in the present paper. The first source is the one associated with the L1551 IRS5 jets, while the two other ones are the sources positionally associated with the L1551 IRS5 molecular outflow but most likely not physically associated with it. The count rate is given in units of counts per ks, while the column "σ" contains the significance of the source detection in the combined MOS+PN image, in units of "equivalent σ" (i.e. obtained by integration of a Gaussian probability distribution). The absorbing column density is given in units of 10^{22} cm^{-2}. For the X-ray source associated with the jets the best fit temperature in MK is given, while for the two sources not associated with the outflows the best-fit power-law index is given. The last column gives the (unabsorbed) X-ray flux in the 0.3–5.0 keV band in units of 10^{-13} erg cm^{-2} s^{-1}.

Source	α	δ	rate	σ	N(H)	T	$F_{\rm X}$
XMM J043134.0 + 180806	04 31 34.0	18 08 06	0.8 ± 0.3	18.0	1.4 ± 0.4	4 ± 2.5	1.3
Source	α	δ	rate	σ	N(H)	γ	$F_{\rm X}$
XMM J043126.9 + 180756	04 31 26.9	18 07 56	3.4 ± 0.3	24.6	2.3 ± 0.7	2.0 ± 0.5	0.7
XMM J043123.4 + 180805	04 31 23.4	18 08 05	3.0 ± 1.4	12.2	1.0 ± 0.3	2.6 ± 1.0	0.6

absorbing column density and the lack of high-energy photons in the spectrum) – emanate from (or close to) the photosphere/chromosphere of the protostars powering the jet. We therefore draw the conclusion that this source is the result of thermal emission in the shocks whose recombination light is seen along the jet in the visual wavelength regime.

The brightest shock as observed in several spectral lines at visual wavelengths (Hα, Hβ, [O III], [O I] and [S II]) is the working surface (knot D – see above). This is also the only position along the jet where [O III] 5007 Å emission has been unambiguously detected (Cohen & Fuller 1985; Sarcander et al. 1985). This is thus indicative of shock velocities $\gtrsim$100 km s^{-1} (Hartigan et al. 1987). At this position the FWZI (Full Width at Zero Intensity) of the Hα emission line is 215 km s^{-1}, while the peak radial velocity is -180 km s^{-1}. Taken together with the proper motion of this knot of $\simeq$200 km s^{-1} (Fridlund & Liseau 1994) this is indicative of a fluid velocity of $\simeq$270 km s^{-1}, and an inclination, $i \simeq 45$ deg. Following e.g. Hartigan et al. (1987) we will assume that the FWZI of the radial velocity is equivalent to the shock velocity, which is also compatible with the presence of relatively strong [O III] emission from this point. From the result of Fridlund & Liseau (1998) we also know that the shock interface is extremely narrow – less than the spatial resolution of HST, which is estimated to be $\leq 1.0 \times 10^{14}$ cm. The immediate post-shock temperature can be estimated as in Raga (1989):

$$T_{\rm ps} \simeq \frac{2.9 \times 10^5 \ {\rm K}}{1+X} \times \left(\frac{v_{\rm shock}}{100 \, {\rm km \, s^{-1}}} \right)^2 \quad (1)$$

where X is the hydrogen pre-ionization fraction and a number abundance of 0.9 (H) and 0.1 (He) has been assumed. Fridlund & Liseau (1998) have found that it is likely that the ionization fraction is close to 1. Then, for a shock velocity of 215 km s^{-1} the resulting temperature will be $T_{\rm ps} \gtrsim 0.67$ MK, somewhat lower than the observed X-ray temperature of 4 ± 2.5 MK. Thus, the observed X-ray emission is likely to be due to material heated at the interface shock (the working surface) between the jet and the ambient medium medium, or possibly in shocks along the cavity excavated by the jet.

The X-ray luminosity of the emission associated with the jets is $L_{\rm X} \simeq 3 \times 10^{29}$ erg s^{-1} (assuming a distance of 140 pc for the L1551 complex). This value is approximately an order of magnitude higher than the Hα-luminosity of knot D, which is $\simeq 4 \times 10^{28}$ erg s^{-1} (Fridlund & Liseau 1994).

6.1. Energetics

Following Fridlund & Liseau (1998), we can attempt to determine the mass and energetics of the jet, and compare these with the X-ray result. From the [S II] 6717/6731 Å ratio we find that the electron density is $n_{\rm e} \simeq 500$ cm^{-3} along the jet, while knot D – identified as the working surface by Fridlund & Liseau (1998) – has an electron density of $n_{\rm e} \simeq 10^4$ cm^{-3}. The ionization fraction in the jet is close to 1 from the reasoning of Fridlund & Liseau (1998).

We assume that the jet consists of the following components: a) a "pipe flow" of $1 \times 1 \times 10$ arcsec geometrical size and density $n_{\rm e} \simeq 500$ cm^{-3} and b) a "working surface" of $2 \times 2 \times 2$ arcsec geometrical size and density $n_{\rm e} \simeq 10^4$ cm^{-3}. Under these assumptions the mass of the jet is then found to be between 1×10^{-6} $M_\odot$ and 2×10^{-6} $M_\odot$ (see also the detailed discussion in Fridlund & Liseau 1998). The shock velocity is $\simeq$200 km s^{-1} from the arguments above, and the highest and lowest fluid velocities (measured proper motions and $v_{\rm rad}$ corrected for inclination) are $\simeq$100 km s^{-1} and $\simeq$300 km s^{-1} respectively. This means that the mechanical luminosity of the jet will be between 10^{41} and 10^{42} erg s^{-1}, so that a very low conversion efficiency between mechanical and radiant luminosity is sufficient to justify the observed X-ray luminosity from the shock. Again, the Hα luminosity is $\simeq 4.7 \times 10^{28}$ erg s^{-1} (Fridlund & Liseau 1998; Fridlund & Liseau 1994), approximately an order of magnitude lower the X-ray luminosity derived here.

A characteristic size for the X-ray emitting region can be derived from the emission measure determined from the X-ray spectrum and the density determined above. The emission measure is defined as $EM = \int n_{\rm e} n_{\rm H} {\rm d}V \simeq 0.8 \, n^2 \, V$, where $n_{\rm e}$ is the electron density, $n_{\rm H}$ the hydrogen density, and V is the volume of the emitting region (under

the simplistic assumption of uniform density). Given that $EM = 1.1 \times 10^{52}$ cm^{-3} (from the thermal fit to the X-ray data), assuming a density $n_e \simeq 10^4$ cm^{-3} (see above), one derives a volume $V = 1.4 \times 10^{44}$ cm^3, which corresponds to a characteristic linear size $l \simeq V^{1/3} \simeq 5 \times 10^{14}$ cm. This scale size is comparable to the upper limit for the size of the shock interface derived from the HST observations, $\leq 1.0 \times 10^{14}$ cm, thus further supporting the identification of the shock interface as the seat of the X-ray emission.

7. Conclusions

While the energetic nature of the collimated jets observed to be originating from protostellar sources has been evident for some time, no high-energy photons have up to now been observed from these phenomena. Here we report the first convincing evidence of X-ray emission from the protostellar jet associated with the IRS5 protostar(s) in the L1551 cloud. The X-ray source and the protostar and related jets are positionally coincident, and the small absorbing column density observed for the X-ray spectrum (with an equivalent $A_V \simeq 7$ mag, fully compatible with the absorbing column density observed in the optical towards the jet) allow us to exclude that the X-ray emission is associated with the protostellar sources (which are hidden behind $\simeq$150 mag of obscuration). The size of the jets ($\simeq$10 arcsec) originating at L1551 IRS5 is smaller in angular extent than the XMM EPIC PSF ($\simeq$14 arcsec), so that no inference is possible on spatial grounds about the possible detailed location of the origin of the X-ray emission.

The emission from the IRS5 jet is compatible with being caused by thermal emission from a plasma heated to a moderate temperature ($T = 4 \pm 2.5$ MK), somewhat higher than the shock temperature that is expected at the interface ("working surface") between the jet and the surrounding circumstellar medium, on the basis of the observed jet velocity. This is regardless of whether it is a bow-shock or a reversed shock, which in itself is a function of whether the jet is denser than the ambient medium or vice versa. Fridlund & Liseau (1998) find strong evidence for the jet being less dense than the surrounding medium. That conclusion was reached by estimating the mass in the jet from the relative brightness of the shock, as well as discerning the ambient density from molecular line measurements. We thus consider it most likely that the X-ray emission originates directly from a shock associated with the so-called knot D.

The presence of a soft X-ray source at the position of the shock associated with the jet is likely to have a significant influence on the physical conditions of the accretion disk: while X-ray emission from the star's corona is often likely to be more powerful that the emission coming from the jet, most of the accretion disk (except for the innermost part) is effectively shielded and not strongly illuminated by the stellar coronal emission. The jet X-ray source on the other hand lies above the disk (if indeed it is located at the jet-circumstellar medium interface it is some 1000 AU above the disk), illuminating the disk from above. This X-ray flux can therefore ionize the disk material, and thus influence significantly the disk physical conditions. Once more, if X-ray emission from protostellar jets is indeed a common feature, this would influence the protostellar environment significantly. This will be investigated in the future through detailed modelling of the relative contribution of the stellar coronal and jet X-ray luminosity to the ionization of the accretion disk.

Acknowledgements. GM, SS acknowledge the partial support of ASI and MURST. This paper is based on observations obtained with XMM-Newton, an ESA science mission with instruments and contributions directly funded by ESA Member States and the USA (NASA). Part of the data have been taken using ALFOSC, which is owned by the Instituto de Astrofisica de Andalucia (IAA) and operated at the Nordic Optical Telescope under agreement between IAA and the NBIfAFG of the Astronomical Observatory of Copenhagen. Nordic Optical Telescope is operated on the island of La Palma jointly by Denmark, Finland, Iceland, Norway, and Sweden, in the Spanish Observatorio del Roque de los Muchachos of the Instituto de Astrofisica de Canarias.

References

Cohen, M., & Fuller, G. A. 1985, ApJ, 296, 620
Cox, A. N. ed. 2000, Allen's astrophysical quantities (Springer)
Damiani, F., Maggio, A., Micela, G., & Sciortino, S. 1997, ApJ, 483, 350
Fridlund, C. V. M., & Liseau, R. 1994, A&A, 292, 631
Fridlund, C. V. M., & Liseau, R. 1998, ApJ, 499, L75
Hartigan, P., Raymond, J., & Hartmann, L. 1987, ApJ, 316, 323
Hasinger, G., Altieri, B., Arnaud, M., et al. 2001, A&A, 365, L45
Neckel, T., & Staude, H. J. 1987, ApJ, 322, L27
Raga, A. C. 1989, in Low Mass Star Formation and Pre-main Sequence Objects, ed. B. Reipurth (European Southern Observatory, Garching bei Munchen), 281
Reipurth, B., & Raga, A. C. 1999, in NATO ASIC Proc. 540, The Origin of Stars and Planetary Systems, 267
Rodriguez, L. F., D'Alessio, P., Wilner, D. J., et al. 1998, Nature, 395, 355
Sandqvist, A., & Bernes, C. 1980, A&A, 89, 187
Sarcander, M., Neckel, T., & Elsaesser, H. 1985, ApJ, 288, L51
Sciortino, S., Micela, G., Damiani, F., et al. 2001, A&A, 365, L259
Smith, H. A., Fischer, J., Schwartz, P. R., & Geballe, T. R. 1987, ApJ, 316, 265
Snell, R. L., Loren, R. B., & Plambeck, R. L. 1980, ApJ, 239, L17
Stocke, J. T., Hartigan, P. M., Strom, S. E., et al. 1988, ApJS, 68, 229
White, G. J., Liseau, R., Men'shchikov, A. B., et al. 2000, A&A, 364, 741